Optical Photometric Evidence for a Binary Black Hole in Mrk 501

L Joseph Rivest III

A senior thesis submitted to the faculty of
Brigham Young University
in partial fulfillment of the requirements for the degree of

Bachelor of Science

Dr. J. Ward Moody, Advisor

Department of Physics and Astronomy

Brigham Young University

June 2017

ABSTRACT

Optical Photometric Evidence for a Binary Black Hole in Mrk 501

L Joseph Rivest III
Department of Physics and Astronomy, BYU
Bachelor of Science

Blazar light curves are studied to deepen our understanding of super massive black hole systems. Sinusoidal variations in a light curve are generally a signature of orbital dynamics. We have made and analyzed optical observations of Markarian 501, using Johnson BVR filters, from 2010–2016. In the optical light curve, we find significant evidence for a sinusoidal variation with a period of ~ 2300 days, or about 6–6.5 years, along with smaller, quasi-periodic variations. In 2000, Rieger & Mannheim calculated a binary black hole orbital period of 6–14 years, based on the 23-day period found in gamma ray observations, by assuming a bulk Lorentz factor $\Gamma = 10$–15 for a helical, relativistic jet, as seen in radio observations. We propose that optical observations reflect the intrinsic orbital period predicted by Rieger & Mannheim and constrain Γ to ~ 10.3. Further investigation could lead to a gravitational wave profile for Mrk 501 and reveal signature characteristics of future candidates for similar gravity wave sources.

Contents

List of Tables

List of Figures

Chapter 1

Introduction

In the literature on Markarian 501 (Mrk 501), there is considerable evidence that its central engine is a binary black hole (BBH). (Begelman et al. 1980; Conway & Wrobel 1995; Komossa 2003; 2006; Villata & Raiteri 1999) The primary motivation for this thesis is that, if the presence of a BBH can be confirmed, then observable characteristics of the host object would give us a window into the internal dynamics of BBHs in galactic nuclei and could be used to identify further BBH candidates. Observations could potentially constrain modeling parameters enough to predict a gravitational wave signal, opening an additional avenue to gravitational wave astronomy.

This first chapter provides general background on blazars and particularly on Mrk 501, the evidence that it contains a BBH, as well as recent developments that may suggest otherwise. This chapter concludes with a brief summary of the work done at BYU as a precursor to this thesis and an overview of my work, which is the subject of chapters 2 and 3.

1.1   Background

Blazars are thought to be super-massive black holes producing a relativistic jet directed towards Earth. There are several theories regarding how the jet formed, but they are generally believed to

be produced by Kerr, or rotating, black holes that have a compact accretion disk. The spin of the black hole drags the magnetic fields around the accretion disk. As charged particles approach the event horizon, they can extract angular momentum from the black hole and accelerate along the rotation axis, forming a bipolar jet. Through this process, the black hole could eventually lose all of its angular momentum, becoming non-rotating, a.k.a. a Schwarzschild black hole. (Wikipedia: Relativistic Jets, Kerr Black Holes, Penrose Process)

BL Lacertae (BL Lac) objects are a subclass of blazar that have observable, rapid and large-amplitude flux variability and significant optical polarization. BL Lac objects have nonthermal spectra dominated by synchrotron radiation and inverse Compton scattering. Jets are formed as electrons are accelerated up to energies above 100 TeV, making BL Lac objects among the most powerful accelerators in the universe. (Ajello et al. 2014)

Markarian 501 (Mrk 501) is a BL Lacertae object hosted by an elliptical galaxy in the constellation of *Hercules*, at a redshift of $z = 0.0337$.(Acciari et al. 2011; Mao 2011) The object of much research on objects like Mrk 501 is to determine the internal dynamics of its central engine. The black hole system is not directly observable, so attempts are made to create a consistent model that cohesively accounts for all the observed traits.

Plotting a celestial body's light curve is a common starting point for much of observational astronomy. Light curves are time-series measurements of the brightness of an object. If a light source is not constant over time, measuring its variational patterns can give insight into the physical process that produces it. One can also plot light curves of the same object in different energy bands, i.e., ranges of wavelengths. This is done by using various telescopes designed to detect light in separate parts of the electromagnetic spectrum. Optical telescopes often have a set of filters to target smaller bands within the optical range. The filter set for our data is called Johnson BVRI, although we mostly only used the B(blue), V(visible), and R(red) filters and not the I(infra-red) filter.

What is observed in the light curves from different energy bands can come from different sources, or components of a source. In the case of Mrk 501, the core should have a thermal, blackbody spectrum, while the jet contains a synchrotron component and a Compton component that up-scatters background photons. For all wavelengths, luminosity is tightly correlated with the core's mass accretion rate. Flares can occur when a large amount of mass suddenly falls onto the black hole or its accretion disk. During a flaring event, the jet also carries a dense emission region known as a knot, shock, electron blob, etc. These are usually observed in high-energy ranges, including X-ray(keV) to TeV. (Acciari et al. 2011) Mrk 501 is also a "radio loud" source, so its jets can be clearly seen in radio wavelengths. (Conway & Wrobel 1995; Komossa 2006; Villata & Raiteri 1999)

1.2   A Binary Black Hole in Mrk 501

Observations of Mrk 501's flaring states show a sinusoidal variation with a 23-day period. (Hayashida et al. 1998; Protheroe et al. 1998; Rieger & Mannheim 2000) This initially gave the idea that something was orbiting the central black hole very closely, perhaps perturbing the accretion disk or varying the mass accretion rate.(Rieger & Mannheim 2000) Radio images of the structure of the jet of Mrk 501 show a peculiarly sharp turn in the path of the jet. Though still unexplained, this phenomenon of orthogonally misaligned jets is not uncommon (Begelman et al. 1980; Komossa 2006). By applying hydrodynamic models, Conway & Wrobel (1995) show that the appearance is indicative of a long helical structure [cf. Figures 1–3 of (Conway & Wrobel 1995) and Figure 2 of (Rieger & Mannheim 2001)] consistent with a BBH central engine. Villata & Raiteri (1999) argue that the evolution of the spectral energy distribution (SED) of Mrk 501 combined with this structure implies a binary with orbital period on the order of years combined with a precession period of the jet axis on the order of 10^4 years, consistent with the driving period found by Conway &

Wrobel (1995). Additionally, according to Croke et al. (2005), a helical, sheath-like magnetic field structure encasing the jet could also explain inhomogeneities across the jet apparent in polarization data.

The BBH model of Mrk 501 attributes the periodicity found in high energy to the jet characteristics found in radio observations. It was championed by Rieger & Mannheim (2000 & 2003, hereafter R&M), who have utilized it in constraining estimates for binary masses, separation, etc. They present a scenario wherein the smaller of the two black holes, $M \sim 6 \times 10^7 M_\odot$, produces the jet while in orbit with the larger, $M \sim 10^8 M_\odot$.

This leads to a clear picture of how we come to observe short-term periodicity in high energy. During a flaring event, the direction of motion of the relativistic 'electron blob' turns towards and away from the line of sight as it follows the helical path of the jet, thus sinusoidally varying the effect of Doppler boosting on the photons it emits (Rieger & Mannheim 2000; 2003; Villata & Raiteri 1999). R&M explain that the same effects behind superluminous motion would cause a theoretical intrinsic variation period of years to appear as days to an observer on Earth. "For a source region which moves in the time interval dt from point A to point B with relativistic velocity v_z and at an angle ψ to the line of sight, the observed difference in arrival times for radiation emitted at A and B is generally given by $dt_{\text{obs}} = dt - dt(v_z/c)\cos\psi$, thus leading to a shortening of the observed time interval." They claim that the 23 day period would correspond to a 6–14 year period for the orbiting black holes, assuming a range of possible inclination angles, which in turn is dependent on a range of the Lorentz factor for the material following the jet: Γ=10-15. For this range, R&M cite Mannheim et al. (1996); Spada et al. (1999) and Hillas (1999).

Hillas (1999) makes a connection between the gamma factor and the magnetic field strength of the jet frame. He explains that Mrk 501, when it was in its highest state in 1997, would have a field strength of 0.03 to 0.1 gauss and a gamma factor of 10-20, but says that the gamma factor could also be more.

Wikipedia gives the only clear explanation I can find for the upper limit of 15, but no source is given. "There is also a jet heading away from the Earth called a counter jet. Close into the core this counter jet is so much dimmer than the main jet that it is invisible in radio waves. The brightness of the counter jet is less than the main jet by a factor of 1250. This implies that the jet is relativistic with Γ about 15 (that is the plasma is moving at 99.8% of the speed of light) and at an angle between $15°$ and $25°$ from the line of sight from the Earth" (Wikipedia: Markarian 501).

1.3   Alternative Models

More recent observations haven't exactly fit nicely into this model. For instance, a multi-wavelength campaign was performed by Rödig et al. (2009) by combining data from several observatories. They find a 72-day period in high-energy data in addition to 36 and 23 day periods, which they suggest are harmonics of the first. They then tie this fundamental period to an intrinsic orbital period according to R&M's model and obtain new BBH mass estimates.

Yang et al. (2007) collected and analyzed optical observations over 30 years. They report two periods in the light curve, 10.06 ± 0.04yr and 21.6 ± 0.17yr, and they point out that 10 years fits in the range of 6–14 years given by R&M. They also find shorter periods that they report to have too high of a false alarm probability (FAP). Their next period with the lowest FAP is 0.31 years, or 113 days.

Giroletti et al. (2004) obtained higher resolution radio images that do not seem consistent with the helical structure postulated by Conway & Wrobel (1995). This leaves an open question on why the jet appears to change direction. They suggest that peculiarities of the jet could be due to interaction with ambient matter, but the bending seen in the jet is too drastic for that to be a likely cause.

Fan et al. (2008) claim that the observed 23 day period could be explained by a single black hole with a two temperature accretion disc creating acoustic instability modes. However, more work would need to be done to reconcile their proposal with observations in optical and radio wavelengths.

1.4 Previous work at BYU

In 2009, Remote Observatory for Variable Object Research (ROVOR) began an optical blazar survey, including Mrk 501. In 2012, the West Mountain Observatory (WMO) began observations of Mrk 501's quiescent state. Marcus Holden and Angel Ritter reduced the optical data from ROVOR(Holden Brigham Young University, 2016). Combining data from ROVOR and WMO, Marcus remarks on the periodicity of the light curve. Since then, Dr. Michael Joner has continued data collection from WMO. We obtained additional data from Dr. Alberto Sadun, but didn't include it due to difficulties of integrating it into our light curve for analysis (cf. Sec. 2.1 and Osborne Brigham Young University, 2017).

1.5 Overview

We have taken and analyzed BVR optical data from 2010-2016 for Markarian 501 and find significant evidence for a sinusoidal variation with a period of ~ 2300 days, or about 6–6.5 years, along with smaller, quasi-periodic variations.

We propose that the model described in R&M accurately reconciles findings from high-energy and optical observations, because the optical observations reflect the intrinsic orbital period predicted by the equations found in R&M, while the high-energy observations exhibit the relativistic effects on which the those equations are based.

Our proposal supports theory that a BBH is present in Mrk 501, because the model is based

upon the helical structure of the jet, which is most likely to be formed by a supermassive black hole that is in orbit with another.

Chapter 2

Data and Analysis

The process of plotting a light curve begins with taking time-stamped images from a telescope. Most of the data in this thesis came from WMO. Raw images from a telescope must be processed before one can accurately measure the brightness of a particular source in the image. Details on processing raw telescope data can be found in Holden (Brigham Young University, 2016). There are many methods and software packages for measuring and plotting relative brightness, or magnitude, from images to form a light curve. Useful information concerning these is available in Osborne (Brigham Young University, 2017) and Hallum (Brigham Young University, 2017). In the following section, I describe the tool I primarily used to create the light curves of Mrk 501 displayed in this thesis. In section 2, I describe the way I used a software package, Period04, to look for sinusoidal periods in the B, V, and R light curves.

2.1 Creating a Light Curve

VPhot can be described as 'photometry as a service' available online. It can be accessed by logging in to AAVSO.org and going to Data>Data Analysis>VPOT.

AAVSO username: astromoody

password: Arcturus

VPhot provides temporary storage space for upload-able images and many tools to help the user produce clean results. Results can then be either downloaded from the Analysis Log or permanently stored in the AAVSO database by making an AAVSO report. Your data can be viewed or downloaded from AAVSO by going to Data>Data Access>WebObs. Users can also download data from other contributors to AAVSO, though they are often difficult to incorporate or rely upon. I tried some frequency analysis with data from James Robert (observer code JM), but eventually threw it out, because its errors and offset were unknown.

The first helpful feature of VPhot is plate-solving the images, which occurs upon uploading. Being plate-solved means VPhot is able to match up the pixel axes of the image with the World Coordinate System (WSC) of the sky. In other words, it can tell you the RA and Dec at each pixel. Two main things are necessary for this to be possible. First, VPhot needs details about your telescope, which must be saved in your account information. Second, the image header (information about the image included in the .fits image file) needs to contain a set of keywords labeled 'CDELT'. Many of the images from WMO come with this information, but some do not. This information can be added to the header by uploading the image to Astrometry.net, which produces a 'new-image.fits' file that you can download and then upload to VPhot. Note that if parentheses are added to the file name as a result of multiple downloads, they must be renamed, as VPhot does not load files having names containing parentheses into its processing queue.

Log in to Astrometry.net through Yahoo!mail— username: astromoody

password: Markarian501

When an image is plate-solved, VPhot can identify background stars in the image that have a catalogued, constant magnitude. After opening an image in VPhot, you can select the target of the image. The catalogue stars can be loaded onto the image as comparison stars. And lastly, VPhot needs the user to select at least one 'Check Star' aside from the comparison stars. With aperture
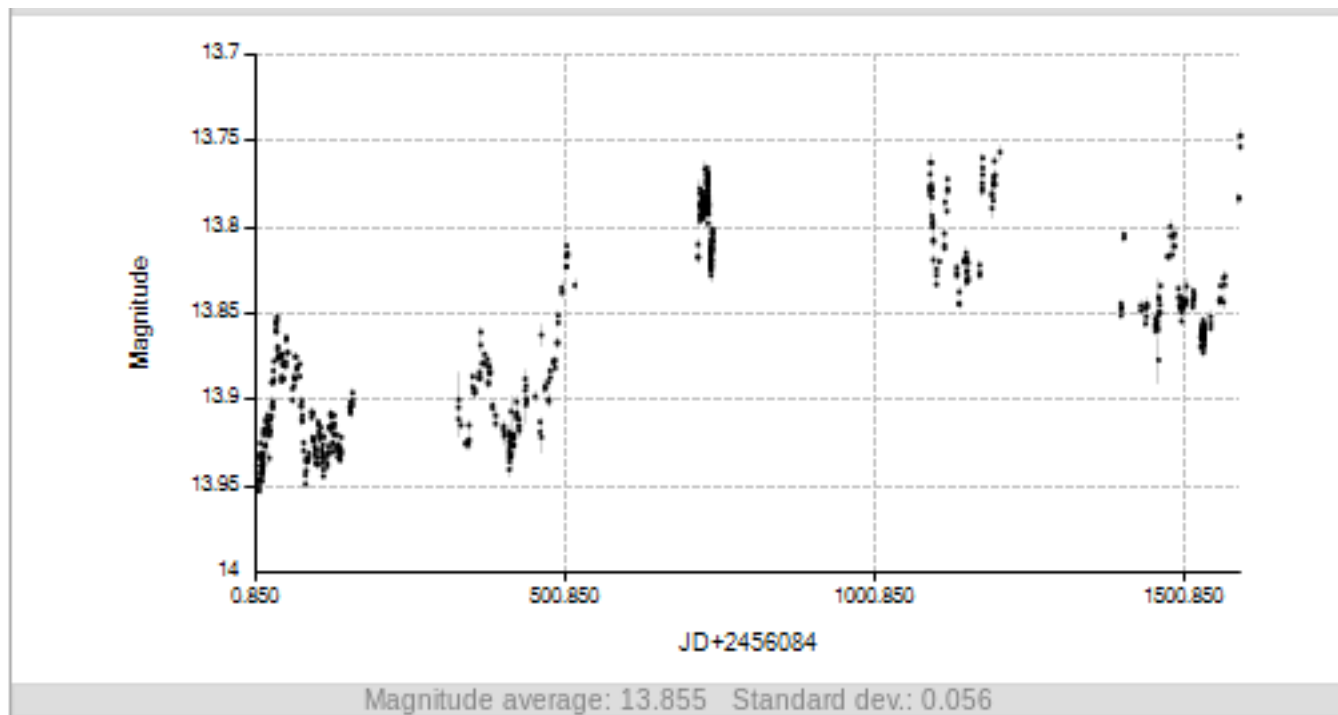
Figure 2.1 WMO V filter light curve of Mrk 501 2012–2016 produced by VPhot.

sizes selected for each object in the image, photometry can be performed instantly by clicking the 'perform photometry' button. The photometry results page not only provides you with a measured magnitude for the target and check stars with accompanying error bars, but it also shows you the effect of the various comparison stars on the measurement—more is not always better. From this page the user can recalculate the magnitudes with selected comparison stars deactivated, until the lowest error is achieved.

The relative locations of the selected stars can be saved as a 'star sequence'. VPhot can then find the stars from your sequence in any of your plate-solved images, even if they are not aligned or a few comparison stars are not in the frame. (It is, of course, preferable to have comparison stars that are at least in most of your frames.)

Finally, to produce a light curve, you can select all the data you want to include from your list of images and click 'Time Series'. The images you select must be from the same telescope and

in the same filter. You then select the star sequence from a drop-down list of saved sequences and select an aperture size for photometry. By default, VPhot uses a multiple of the FWHM of the target's radial profile, which means that the aperture size will be adjusted to the apparent size of the object in each image. This is usually ideal for minimizing error for stars. However, Mrk 501 is a galactic core. The host galaxy can be mistaken by VPhot as the background sky, and the aperture size greatly affects how bright the target is measured to be. So instead, as Mrk 501 gets brighter and dimmer, VPhot needs to use a fixed aperture size that fully encompasses the core, in order to see the full amplitude of the variations. The aperture size is set be a pixel radius, but the number of pixels covered by the core depends on the plate scale of the telescope. For example, the aperture size most commonly used for Mrk 501 is 5", and the plate scale for WMO is 0.61"/pixel, so I set the aperture size for the Time Series to 8.2 pixels. This produced the V filter light curve shown in Fig.2.1. The light curves for R and B show all the same dips and peaks, but they are shifted showing that Mrk 501 is brighter in R and dimmer in B.

VPhot has some limitations when it comes to handling large amounts of data. When the Image List on the home page gets to around 7000 images, it'll crash trying to load them all. Fortunately, there are ways to select which images to include in the list, and default display is only the most recently uploaded. Creating a time series starts taking a long time when it includes 500–800 images and could crash if there's more than 1000. This can be handled by making a series of time series, i.e., breaking it up into segments. Another helpful trick is to either randomly include or randomly exclude some fraction of images, especially when there are periods of unnecessarily dense sampling. How many images can be uploaded at once depends on the day, ranging from roughly 10 to 80. However, uploading puts the images in the processing queue which is shared with whoever has their accounts on that particular server, and processing is done first-come-first-serve. Also, if a file is uploaded to the queue with the same name as another, it will replace the first one and take its place in line.
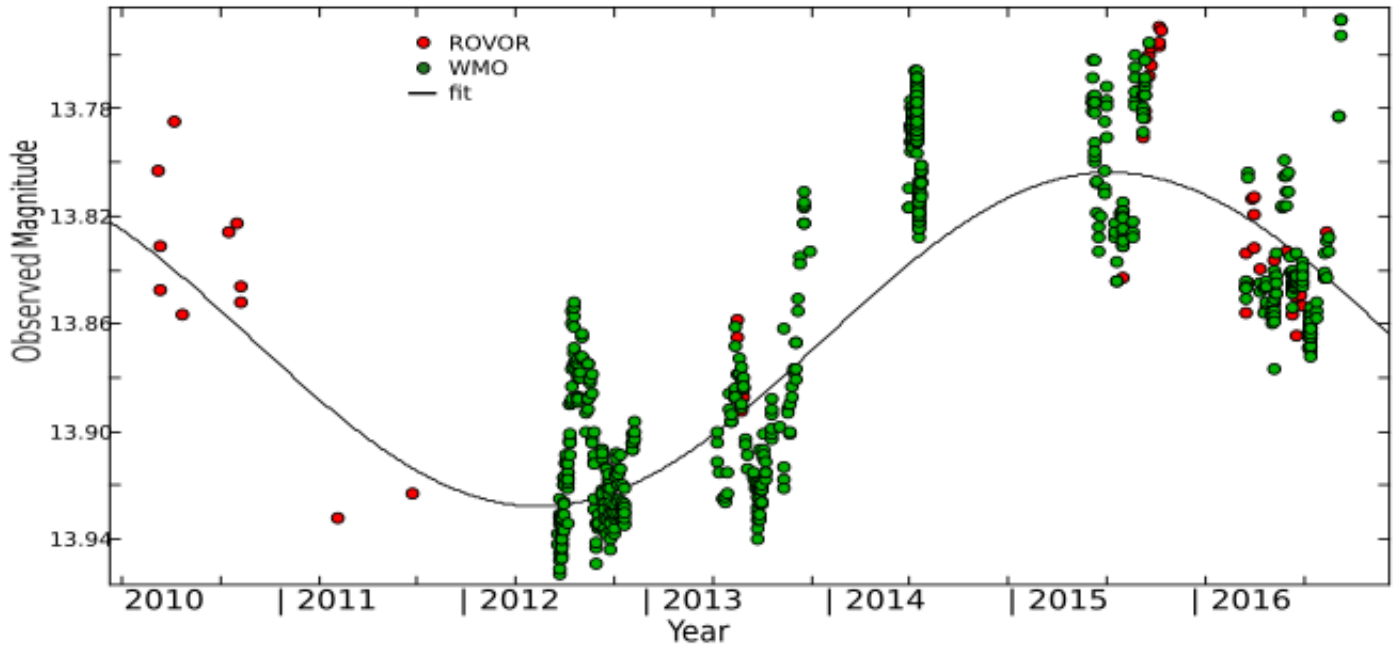
Figure 2.2 Light curve, created using Period04, of Mrk 501 in the V filter collected by ROVOR (red dots) and WMO (green dots) during observable seasons in 2010–2016. A fitted sinusoid having a 2318 day period and amplitude of ~ 0.06 mag is overlaid.

2.2 Frequency Analysis

Unlike other forms of signal processing, data in a light curve are not evenly sampled with a constant time step. This presents a challenge to standard Fourier transformation analysis. So other methods must be sought. One common method is fitting many frequencies within a range and treating the residuals for each as an effective amplitude for the spectrum. A residual curve is the result of subtracting a wave of a particular frequency and amplitude from every data point. The residual is related to the average deviation from a flat line after subtracting one or more frequencies. Before subtracting a frequency, the 'zero point' or offset needs to be subtracted out.

For this process, I primarily used a software package called Period04 to search for a consistent period in the light curve. After importing a light curve, Period04 has a Fourier tool which allows

you to search for a sinusoidal frequency that gives a first-order approximation to the light curve. Fig. 2.2 displays both the data seen in Fig. 2.1 and data obtained from ROVOR added to the light curve by Osborne (Brigham Young University, 2017). This first frequency can be added to the fit calculator to find the amplitude and phase that give a best fit for that frequency. The first-order fit that Period04 produces for this light curve is shown overlaid in Fig. 2.2. Additional frequencies can be generated from the residuals of frequencies selected in the fit calculator by clicking 'Residuals' (as opposed to using 'Original') and repeating the process. Subsequent frequencies can then be included in the fit calculation. The result can look like Fig.2.3. You can see in these figures how particular frequencies characterize features of the light curve.

Quantifying these features is vital to determining a physical mechanism that accurately models their source. The numeric results from Period04 are fitting parameters, like those in Table 2.1. The fitted curve $y(t)$ [*mag*], like those in Figs.2.2 and 2.3, is calculated with the equation $y(t) = Z + \Sigma_i\, A_i\, sin(2\pi(t/P_i + \Phi_i))$. The fitting parameters are as follows: Z is the zeropoint or offset magnitude; P_i indicates the i-th period in the list; A_i is the amplitude of the i-th term in magnitudes, and Φ_i is its phase shift. The time t is in days and takes the Julian Date.

My goal was to find the fewest frequencies necessary to make a best fit with small residuals. I could then note any differences in the results from each filter. Like in Table 2.1, I restricted the fitting formula to four terms and selected the frequencies that gave the lowest residuals and were common between the three filters, Johnson B, V, and R. In each filter, the S/N becomes too low at the fourth frequency. It is important to note that the particular results in this table is an example of what can be exported from Period04 for our data. The particular numbers may be able to vary and yet give an equally good fit.

A very close match is to be expected between optical filters, because we are assuming a single blackbody curve as the source of variation. Often, it is necessary to replace several frequencies produced by Period04 with one or two that clearly give a good fit for certain years. This sort of

Figure 2.3 V filter light curve from WMO exported from Period04. The fitted curve uses three terms with parameters similar to those in Table 2.1 for the V filter. The colors represent data in the years 2012(green), 2013(dark blue), 2014(light blue), and 2015(yellow), and appear because I subdivided the time string. This plot does not include the data from 2016.
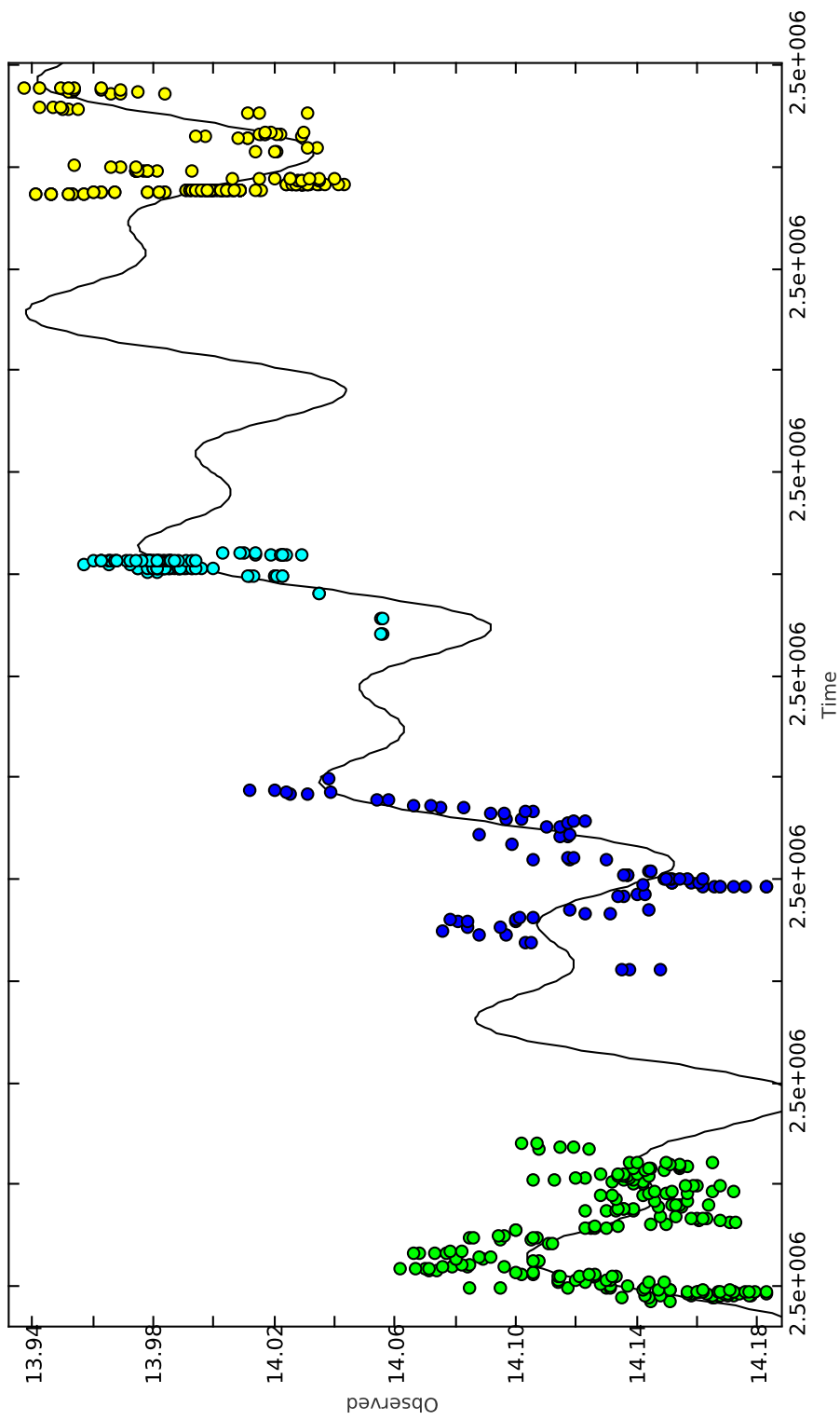
testing allows the user to compare the impact that different combinations of frequencies have on the residuals.

Another important feature is that the user can select certain parameters to hold constant and have Period04 recalculate the others. In the initial calculation, the frequencies are held constant, while the amplitudes and phases are varied. You can also divide the light curve into several time strings and then perform calculations with only certain time strings. Because data from ROVOR is not as well sampled as the WMO data, I only included it when determining the long-period term. I would then select only the WMO data and have the shorter-period terms recalculated, with the

Table 2.1 Results from Period04. Period04 searches for frequencies to give a first approximation to the light curve, and then allows you to select frequencies to include in the fitting formula. It is important to note that the particular results in this table is an example of what can be exported from Period04 for our data. The particular numbers may be able to vary and yet give an equally good fit. For this table, I selected frequencies found for the V light curve that were similar to those found for B and R, and then inserted them into the fit calculator for the R and B light curves, which were open in separate windows on the desktop.

Z is the zeropoint or offset magnitude of Mrk 501 in a particular filter. Fi indicates the i-th frequency, or term, in the list. The frequency is in variation cycles per day, but the number we are interested in is the period $P_i = 1/$Fi. A_i is the amplitude of the i-th term in magnitudes, and Φ_i is its phase shift. The time t is in days and takes the Julian Date. These are used in the fitting formula $y(t) = Z + \Sigma_i A_i \sin(2\pi(t/P_i + \Phi_i))$.

		F_i	$1/P_i \,[day]^{-1}$	$P_i \,[day]$	$A_i \,[mag]$	Φ_i
B Filter	$Z = 14.5753$	F1	0.000433367	2307.513	0.09906	0.86377
		F2	0.0084046	118.982	0.02649	0.40609
		F3	0.0045997	217.405	0.02718	0.95624
		F4	0.0149545	66.870	0.01725	0.59278
V Filter	$Z = 13.8644$	F1	0.000433367	2307.513	0.06241	0.88247
		F2	0.0084046	118.982	0.02117	0.08749
		F3	0.0045997	217.405	0.02580	0.18428
		F4	0.0149545	66.870	0.01068	0.59496
R Filter	$Z = 13.3406$	F1	0.000433367	2307.513	0.05766	0.88195
		F2	0.0084046	118.982	0.01117	0.18060
		F3	0.0045997	217.405	0.01527	0.18800
		F4	0.0149545	66.870	0.00628	0.64887

long-period term held constant. Further insight can be gained by calculating a fit for a particular time string(s), or years in the light curve, to see how well it predicts the rest of the light curve.

Period04 is originally meant for identifying frequencies in δ-Scuti stars and other variable stars; thus it is more suited towards well sampled light curves with variations measured in cycles-per-day, rather than days-per-cycle (Hintz 2016). Because we are studying a much larger-scale structure, the internal dynamics are more chaotic and their light curves are naturally 'noisier'. Additionally, the dynamics we are hoping to uncover occur on much longer timescales. Thus, a meaningful analysis requires several years of observations in order to obtain statistically significant results.

Confidence in a particular frequency is expressed as the Signal-to-Noise ratio, S/N, at that frequency. For Mrk 501, changes in magnitude appear on all timescales from minutes (Xiong et al. 2016) to decades (Yang et al. 2007). But, when optimizing a fitted curve, the amplitude (signal) and the consistent timing (periodicity) of flux variations both seem to scale naturally with the length of the period being fitted. However, the natural spread of the data, i.e. the noise, has a nearly constant amplitude – like ~ 0.01mag in the V filter. I, therefore, have a range of frequencies to tell Period04 to search within, and I can rule out frequencies that appear with an amplitude that is too small compared to the residuals. Frequencies under $\sim 0.00037[day]^{-1}$ equate to a period too long compared to the span of our data (7.5 year period versus 6 years of data). Frequencies greater than $\sim 0.0125[day]^{-1}$ (or a period less than 80 days) begin to cause aliasing.

Aliasing also occurs when too many terms are applied. Period04 begins to give frequencies with erroneous amplitudes or repeats of a frequency with different phase shifts. This trend becomes more apparent when the number of terms increases beyond about five. However, sometimes important frequencies are generated only after a few repeats and high frequencies, so it is important in an initial search to generate several frequencies, and then eliminate the extraneous ones.

Additional challenges arise from the uneven sampling of data. For example, in 2012, we almost almost exclusively observed in the V filter. Patterns in the timing and number of images per night

varied greatly as different students used the telescope. Periods of denser sampling contribute more to the residuals, and thus tend to dominate the fit. This benefits us in that more weight is given to features where there is more confidence in the average value. But when the difference is drastic—as in hundreds of points in a particular day or thousands in a few particular weeks, as opposed to a quasi-steady rate of two to six per day for several days per month—the rest of the light curve gives negligible residuals, even where enough data is present to give confidence to visible features.

Some methods we thought of for navigating this involve replacing several data points with one representing their average value. One example is stacking images in VPhot, as described in Sec.2.1. Methods of data reduction used for our light curve are discussed in Osborne (Brigham Young University, 2017). In Period04, there are two tools in the "Special" menu that can be help in this situation. One is subdividing the time string(light curve), as mentioned earlier, so that you can perform frequency analysis one or more particular segments of the light curve. The other is weight selection, which allows you artificially weight certain data points more than others. Period04 also allows the users to set aside individual data points into a 'deleted points' list, which acts as a separate time string. Points are added to this list by manually selecting them from the list or by boxing them on the graph with a right-mouse-click (be careful about zooming in too far to do this, as it could crash the graph window).

Of course, more details of how to use Period04 is available in the 'Help' documentation for the program. A few other features I've explored, and found some use for are adjusting data, calculate noise at frequency, and all the buttons immediately visible in each tab.

Chapter 3

Results and Conclusions

The first section in this chapter summarizes the conclusions I've drawn from the results I've attained from Period04. These become key in the discussion portion of section 3.2, where I explain why my results, combined with information gathered from the literature, provide evidence that Mrk 501 has a BBH. I then conclude with a summary of my conclusions and further work it could lead to.

3.1   Data Analysis

While an exact fit for short term variation is not expected, frequency analysis of these light curves consistently show that the best fit with the fewest terms is roughly given by a linear combination of three periods in the ranges of 95–120, 200–240, and 1900–2400 days (see Table 2.1). In fact, it appears that variations in the lower two ranges tend to evolve between their extremes over time. More details of these results can be found in Osborne (Brigham Young University, 2017). The 113 day period found by Yang et al. (2007) (see Chap. 1) appears in our data with a similar confidence level, but this is the only match. The amplitudes of the variations in our light curve are larger in the B filter than in V and R, showing that Mrk 501 is "bluer-when-hotter", which also agrees with

18

Yang et al. (2007).

Several individual variations on the order of 30 days are evident during weeks of more consistent sampling, but we are unable to make a match for all of these variations in one fit, even with as many as ten terms. Three densely sampled days were used to search for any intra-day variations. No such short-term periods were found. The rest of the data was too sparse to detect periods shorter than 15 days, without aliasing, due to the natural spread of the data.

Very short-term variations are likely to appear, however. For example, Xiong et al. (2016) looked for short-term changes in the optical magnitude of Mrk 501 and report variations on a minimal timescale of 106 minutes. But, no attempt is made to say that these variations are periodic, let alone sinusoidal.

Also, Yang et al. (2007) report a delay of 1.2–1.6 years from B-band to radio. Through polynomial fitting in another program, called Peranso, we've estimated that the B curve leads R by 1 ± 1 days, which is not statistically significant.

3.2 Evidence for a Binary Black Hole Model

3.2.1 Discussion

In considering the relativistic effects described in Chap. 1, Reiger and Mannheim (2000) derive an equation for converting a light curve period P_{obs} observed in the jet to an intrinsic orbital period P_k for a theoretical binary companion that forms the helical jet.

$$P_{\text{obs}} \simeq (1+z)\left(1 - \sqrt{1 - \frac{1}{\Gamma^2}}\cos\left(\Gamma^{-1}\right)\right)P_k \tag{3.1}$$

For Mrk 501, the redshift is z = 0.0337 (see Sec. 1.1). Most literature use the range Γ=10–15 (Rieger & Mannheim 2000; Rödig et al. 2009) for the bulk Lorentz factor for the outflow velocity,

the basis being $\Gamma \simeq 10$ from Mannheim et al. (1996); Spada (1999); Spada et al. (1999), $\Gamma \gtrsim 10$ from Hillas (1999), and $\Gamma \simeq 15$ from Mannheim et al. (1996); Spada et al. (1999)(cf. Sec. 1.2). Inserting this range into Eq. (3.1) maps the observed period of 23 days to P_k=6.1–13.7yrs, as reported by R&M.

In our analysis, it will be useful to define the ratio P_k/P_{obs}.

$$\frac{P_k}{P_{\text{obs}}} = \left((1+z) \left(1 - \sqrt{1 - \frac{1}{\Gamma^2}} \text{Cos}\left[\Gamma^{-1}\right] \right) \right)^{-1}$$

$$\frac{P_k}{P_{\text{obs}}} = 96.9012\text{–}217.826$$

(3.2)

Rödig et al. (2009), in a multi-wavelength campaign, find periods in X-ray to 10 TeV observations of 72, 36, and 23 days and suggest that 72±4.3 days is the fundamental period, while 36 and 23 day periods arise as harmonics.

If the observed period is now 72 days, then naturally Eq. (3.1) and Eqs. (3.2) give us a new intrinsic orbital period, and the harmonics might also follow.

$$72 \text{ days} \times \frac{P_k}{P_{\text{obs}}} \frac{1 \text{ yr}}{365.25 \text{ days}} = 19.1017\text{–}42.939 \text{ yrs}$$

$$36 \text{ days} \times \frac{P_k}{P_{\text{obs}}} \frac{1 \text{ yr}}{365.25 \text{ days}} = 9.55083\text{–}21.4695 \text{ yrs}$$

$$23 \text{ days} \times \frac{P_k}{P_{\text{obs}}} \frac{1 \text{ yr}}{365.25 \text{ days}} = 6.10192\text{–}13.7166 \text{ yrs}$$

(3.3)

Rödig et al. (2009) did include some data from the Ultraviolet/Optical Telescope on the SWIFT satellite. However, the optical data they had contradicted their conclusion, but it was too sparse and too noisy to contribute to their analysis.

Yang et al. (2007) reported optical variation periods in order of lowest False Alarm Probability: 10.06, 21.6, 0.31, 0.37, 0.42, 0.3. And in our light curve, we find a prominent 6.5 year period. Notice that their two most confident periods have very similar ratios with our period as the harmonics

from Rödig et al. (2009):

$$\frac{21.6 \text{ yrs}}{6.5 \text{ yrs}} = 3.32308 \quad \text{and} \quad \frac{10.06 \text{ yrs}}{6.5 \text{ yrs}} = 1.54769$$

$$\text{compared to} \quad \frac{72.6 \text{ days}}{23 \text{ days}} = 3.15652 \quad \text{and} \quad \frac{36 \text{ days}}{23 \text{ days}} = 1.56522 \, . \tag{3.4}$$

This similar behavior between the optical observations in the top line and the high-energy observations in the bottom line hint at a relationship between the mechanisms producing them. Optical variations should lack the relativistic effects seen in high-energy, because they are emitted from the core, rather than the jet. So, this correlation could be the same relationship R&M defined for P_k and P_{obs}.

I can test the correlation between the high-energy data and the optical data by the following method: (1)Replace the theoretical intrinsic period, P_k, in Eq. (3.1) with the periods observed in optical; (2)Then, numerically solve for Γ; (3)And then compare that value to the possible values for Γ from the literature. I performed this analysis in Mathematica; my code and commentary can be found in Appendix A. The result is that the observations in high-energy and optical are in very close agreement with the equations of R&M's model when the Lorentz factor is constrained to $\Gamma = 10.3^{+0.3}_{-0.15}$.

3.2.2 Summary

Most evidence for alternative models don't consider the observed long-term variations. The model put forth by R&M predicts an agreement between non-thermal, high-energy observations and optical, intrinsic variations. The best fits to our optical (Johnson BVR) light curves give periods in the range 2300 to 2400 days. By R&M's equations, I propose that the bulk Lorentz factor of the relativistic jet during the time of our observations falls in the range of $\Gamma \simeq 10.159$–10.334 and that the period we've observed is intrinsic to the AGN and corresponds to the 23 day period observed

in high energy. Furthermore, if the harmonics reported by Rödig et al. (2009) follow the modeled relationship put forward by R&M, then a Γ of ~ 10.3 relates them to intrinsic periods of roughly 20.3, 10.1, and 6.5 years, which very closely match the periods found here and by Yang et al. (2007).

Bon et al. (2016) found a similar pattern for NGC 5548, where a clear long-term variation appears with additional short-term variations visible. This similarity suggests a common origin for their light curves. Further investigation could lead to a model constrained enough to predict a gravitational wave profile for Mrk 501 and reveal signature characteristics of future candidates for similar gravity wave sources.

3.3 Directions for Further Work

Probably the most important question from here is whether or not the presence of harmonics makes physical sense in the helical jet and BBH model. Could an internal mechanism produce harmonics in optical that follow the relationship from R&M? One possibility is that the magnetic field strength varies according to the mass accretion rate of the BBH, similar to the intensity of thermal emissions. The specific orbital mechanics could give rise to orbital resonances, migrating rings of mass, etc., leading to periodic variations in the mass accretion rate of the jet-forming component of the BBH.

Continued observations from WMO will give clearer results. Further study and ingenuity will be needed to further develop methods for using Period04, and another program called Peranso, to more thoroughly investigate short-term variations. One particular point of interest is the way the short-period terms change from year to year, in both amplitude and frequency. I recently found these useful sources for utilizing Period04: Fu et al. (2014); Lenz & Breger (2004; 2005).

It will be important to keep up with new literature for all wavelengths of observations and

models of Mrk 501, both to understand the physics and to compare other data and predictions to our light curve. For example, Fan et al. (2008), from their model(see Chap. 1), predict a period variation of $\Delta P/P \sim .23$, which might fit our 95-120 and 1900-2400 ranges. They also refer to shorter variations on the 23 day period of 5-15 hours, and I calculated that variation to correspond to 20-60 days, assuming Γ=10. This could potentially explain features in the like curve (see 2.3) that are difficult to match in the Fourier solution, such as the drifting of short-term periods over the 2014 gap. More analysis on these points is done in the Additional Notes section of Appendix A.

Appendix A

Mathematica Code

Reiger and Mannheim (2000) derive an equation for converting a light curve period, P_{obs}, observed in the jet to an intrinsic orbital period, P_k, for a theoretical binary component forming the helical jet.

Eq.(1): $P_{obs} \simeq (1+z)\left(1 - \sqrt{1 - \frac{1}{\Gamma^2}} \cos\left(\Gamma^{-1}\right)\right) P_k$

This is Eq. (3.1) in the text. For Mrk 501, the redshift is z = 0.0337. We use Γ=10–15 for the bulk Lorentz factor.

It is useful to define the ratio P_k/P_{obs}.

In : $z = 0.0337; \text{Pratio} = \left((1+z)\left(1 - \sqrt{1 - \frac{1}{\Gamma^2}}\text{Cos}\left[\Gamma^{-1}\right]\right)\right)^{-1} /.\Gamma \to \{10, 15\}$

Out : $\{96.9012, 217.826\}$

Rodig *et al*. (2009), in a multi-wavelength campaign, find periods in X-ray to 10TeV observations of 72, 36, and 23 days and suggest that 72±4.3 days is the fundamental period, while 36 and 23 day periods arise as harmonics.

If the observed period is now 72 days, then naturally Eq.(1) gives us a new intrinsic orbital period.

In : $72 * \text{Pratio}/365.25\text{"yrs"}$

Out : $\{19.1017\text{yrs}, 42.939\text{yrs}\}$

The harmonics might also follow.

In : $36 * (\text{Pratio}/365.25) * \text{"yrs"}$

Out : $\{9.55083\text{yrs}, 21.4695\text{yrs}\}$

In : $23 * (\text{Pratio}/365.25) * \text{"yrs"}$

Out : $\{6.10192\text{yrs}, 13.7166\text{yrs}\}$

The reported optical periods from Yang *et al*. (2007) in order of lowest False Alarm Probability, converted from years to days, are:

In : $\text{Yang} = \{10.06, 21.6, .31, .37, .42, .3\} * 365.25$

Out : $\{3674.42, 7889.4, 113.228, 135.143, 153.405, 109.575\}$

In our light curve, we find a prominent 6.5 year period. Notice that the most confident periods have very similar ratios with our period as the harmonics from Rodig *et al.* (2009).

In : $\{21.6, 10.06\}/6.5$

Out : $\{3.32308, 1.54769\}$

In : $\{72.6, 36.0\}/23$

Out : $\{3.15652, 1.56522\}$

This similar behavior in relativistic, high-energy observations and non-relativistic, optical observations hint at a relationship between the mechanisms producing them. If so, it might be the same relationship R&M defined for P_k and P_{obs}. To test this, I replace the theoretical intrinsic period, P_k, with periods observed in optical in order to constrain Γ.

In our light curve, a period for a one-term fit is probably between 1900–2500 days; a fit using less than 1900 days overshoots the 2010 data and undershoots it when using more than 2500 days—the WMO data is always closely matched, because it has much denser sampling (see Sec. 2.2).

In : $\mathbf{Pobs1 = 23; Pobs2 = 36; Pobs3 = 72.6; (*Pk=\#*)}$ – Define variables.

$\mathbf{FindRoot[1 - Pobs1/((1+z)\#)==Sqrt[1 - \Gamma^{\wedge}(-2)]Cos[1/\Gamma], \{\Gamma, 10\}]\&/@}$

$\{1900, 2200, 2300, 2400, 2500\}$ – What must Γ be if 23 days corresponded with these values for P_k?

Out : $\{\{\Gamma \rightarrow 9.23179\}, \{\Gamma \rightarrow 9.93524\}, \{\Gamma \rightarrow 10.1589\}, \{\Gamma \rightarrow 10.3777\}, \{\Gamma \rightarrow 10.5921\}\}$

However, when including the next two significant terms into the fit— 95–120 and 200–240 days —the range for the long-term period narrows to 2300–2400 days. We'll package the extremes of this range with the 10 and 21 year periods and see if Eq.(1) shows coherence between the high-energy harmonics and what might be optical harmonics.

In : $\mathbf{Harmonics = \{2300, 2400, 3674.415, 7889.4\};}$ $\mathbf{(*6.34 - 6.5, 10.06, 21.6years*)}$

$- 23$ days

FindRoot[1 − Pobs1/((1 + z)#)==Sqrt[1 − Γ^(−2)]Cos[1/Γ], {Γ, 10}]&/@Harmonics

Out : {{Γ → 10.1589}, {Γ → 10.3777}, {Γ → 12.8442}, {Γ → 18.8258}}

– 36 days

In : FindRoot[1 − Pobs2/((1 + z)#)==Sqrt[1 − Γ^(−2)]Cos[1/Γ], {Γ, 10}]&/@Harmonics

Out : {{Γ → 8.11635}, {Γ → 8.29136}, {Γ → 10.2635}, {Γ → 15.0456}}

– 72.6 days

In : FindRoot[1 − Pobs3/((1 + z)#)==Sqrt[1 − Γ^(−2)]Cos[1/Γ], {Γ, 10}]&/@Harmonics

Out : {{Γ → 5.708}, {Γ → 5.83139}, {Γ → 7.22154}, {Γ → 10.5908}}

The first three values of Γ for $P_{obs} = 72.6$ are not possible values for the bulk Lorentz factor, since they are significantly less than 10. This confirms that, assuming the model from R&M holds, the 72.6 day period must correspond to the 21 year period and indicates that Γ must be near the value 10.6. Similarly, 36 days corresponds to 10 years, suggesting $\Gamma \sim 10.26$, and 23 days to 6.3–6.5 years, and $\Gamma \sim 10.15$–10.4.

To see how well this new range for the Lorentz factor, $\Gamma = 10.15$–10.6, fits the data, I plug it into Eq.(1) and instead solve for P_k converted to years.

In : FindRoot[1 − Pobs1/((1 + z)Pk ∗ 365.25)==Sqrt[1 − #^(−2)]Cos[1/#], {Pk, 6.5}]&/@

{10.15, 10.2, 10.3, 10.4, 10.5, 10.6} – 23 days

Out : {{Pk → 6.28604}, {Pk → 6.34803}, {Pk → 6.47291}, {Pk → 6.59901},

{Pk → 6.72633}, {Pk → 6.85486}}

In : FindRoot[1 − Pobs2/((1 + z)Pk ∗ 365.25)==Sqrt[1 − #^(−2)]Cos[1/#], {Pk, 10}]&/@

{10.15, 10.2, 10.3, 10.4, 10.5, 10.6} – 36 days

Out : {{Pk → 9.83903}, {Pk → 9.93604}, {Pk → 10.1315}, {Pk → 10.3289},

{Pk → 10.5282}, {Pk → 10.7293}}

In : FindRoot[1 − Pobs3/((1 + z)Pk ∗ 365.25)==Sqrt[1 − #^(−2)]Cos[1/#], {Pk, 21.6}]&/@

{10.15, 10.2, 10.3, 10.4, 10.5, 10.6} – 72.6 days

Out : {{Pk → 19.842}, {Pk → 20.0377}, {Pk → 20.4319}, {Pk → 20.8299},

{Pk → 21.2318}, {Pk → 21.6375}}

These show a very tight coherence, given the error bars reported for the high-energy periods (Rödig et al. 2009).

A.0.1   Additional Notes

Fan *et al*. (2008) predict a period variation $\Delta P/P \sim .23$ and compare their two-temperature accretion disk model to observed variations of 5-15 hours on the 23 day period.

In : TeVvar = {5, 15}/24//N(*Convert hours to days*)

Out : {0.208333, 0.625}

In : TeVvar/23

Out : {0.00905797, 0.0271739}

Here, I search for this predicted variation in our data.

In : max = {78, 120, 240, 2500}; (*High end of our period ranges*)

min = {63, 95, 200, 1900}; (*Low end*)

((max − min))/(min + (max − min)/2)//N

Out : {0.212766, 0.232558, 0.181818, 0.272727}

For another comparison, the ratio between the 72 day period and its error bar is

In : 4.3/72.6

Out : 0.0592287

Here, I find an "intrinsic" counterpart to the 5-15 hours, assuming Γ=10.

In : TeVvar ∗ (6.1 ∗ 365.25)/23

Out : {20.1814, 60.5442}

Bibliography

Acciari, V. A., et al. 2011, ApJ, 729, 2

Ajello, M., et al. 2014, The Astrophysical Journal, 780, 73

Begelman, M. C., Blandford, R. D., & Rees, M. J. 1980, Nature, 287, 307

Bon, E., et al. 2016, ApJS, 225, 29

Conway, J. E., & Wrobel, J. M. 1995, ApJ, 439, 98

Croke, S., Charlot, P., Gabuzda, D., & Sol, H. 2005, Baltic Astronomy, 14, 367

Fan, J. H., et al. 2008, Astroparticle Physics, 28, 508

Fu, J., Zhang, X., & Xiong, D. 2014, Journal of Astrophysics and Astronomy, 35, 279

Giroletti, M., et al. 2004, ApJ, 600, 127

Hallum, M. Brigham Young University, 2017, Senior Thesis

Hayashida, N., et al. 1998, ApJ, 504, L71

Hillas, A. M. 1999, Astroparticle Physics, 11, 27

Hintz, E. 2016, Private communication

Holden, M. Brigham Young University, 2016, Senior Thesis

Komossa, S. 2003, in American Institute of Physics Conference Series, Vol. 686, The Astrophysics of Gravitational Wave Sources, ed. J. M. Centrella, 161–174

Komossa, S. 2006, Mem. Soc. Astron. Italiana, 77, 733

Lenz, P., & Breger, M. 2004, in IAU Symposium, Vol. 224, The A-Star Puzzle, ed. J. Zverko, J. Ziznovsky, S. J. Adelman, & W. W. Weiss, 786–790

Lenz, P., & Breger, M. 2005, Communications in Asteroseismology, 146, 53

Mannheim, K., Westerhoff, S., Meyer, H., & Fink, H.-H. 1996, A&A, 315, 77

Mao, L. S. 2011, New A, 16, 503

Osborne, M. Brigham Young University, 2017, Senior Thesis

Protheroe, J., Bhat, C. L., Fleury, P., Lorenz, E., Teshima, M., & Weekes, T. C. 1998, International Cosmic Ray Conference, 8, 317

Rieger, F. M., & Mannheim, K. 2000, A&A, 359, 948

Rieger, F. M., & Mannheim, K. 2001, in American Institute of Physics Conference Series, Vol. 558, American Institute of Physics Conference Series, ed. F. A. Aharonian & H. J. Völk, 716–720

—. 2003, A&A, 397, 121

Rödig, C., Burkart, T., Elbracht, O., & Spanier, F. 2009, A&A, 501, 925

Spada, M. 1999, Astroparticle Physics, 11, 59

Spada, M., Salvati, M., & Pacini, F. 1999, ApJ, 511, 136

Villata, M., & Raiteri, C. M. 1999, A&A, 347, 30

Xiong, D., Zhang, H., Zhang, X., Yi, T., Bai, J., Wang, F., Liu, H., & Zheng, Y. 2016, ApJS, 222, 24

Yang, J. H., Fan, J. H., Liu, Y., Wang, Y. X., & Yang, Y. S. 2007, Acta Astronomica Sinica, 48, 407

Index